International Journal of Bifurcation and Chaos, Vol. 24, No. 9 (2014) 1430025 (17 pages)

DOI: 10.1142/S0218127414300250

The Negative Side of Chua's Circuit Parameter Space: Stability Analysis, Period-Adding, Basin of Attraction Metamorphoses, and Experimental Investigation

Rene O. Medrano-T
Federal University of São Paulo – UNIFESP/DCET,
Campus Diadema, 09972-270, Diadema, SP, Brazil
rmedrano@if.usp.br

Ronilson Rocha
Federal University of Ouro Preto – UFOP/EM/DECAT,
Campus Morro do Cruzeiro, 35400-000, Ouro Preto, MG, Brazil
rocha@em.ufop.br

Received November 19, 2013; Revised March 22, 2014

Although Chua's circuit is one of the most studied nonlinear dynamical systems, its version with negative parameters remains practically untouched. This work reports an interesting and rich dynamic scenery that was hidden in this almost unexplored region. The study is focused on 2D parameter space and presents an analysis of stability based on describing functions. Numerical investigations present a gallery of period-adding cascades and a strong presence of basin boundary metamorphoses. The key to this new scenario is that for negative parameters, Chua's system does not satisfy the Shilnikov condition and it is shown that the homoclinic orbit organizes the parameter space completely different from as known. The obtained experimental results corroborate with the numerical and theoretical investigations.

Keywords: Chua's circuit; period-adding; basin boundary metamorphoses; homoclinic bifurcation; describing functions.

1. Introduction

Chua's circuit is a paradigm in nonlinear dynamics and has been extensively studied since 1984 [Matsumoto, 1984]. This simple electric circuit presents a dynamics with a wide diversity of attractors [Matsumoto, 1984; Matsumoto *et al.*, 1987], a strictly proven chaotic behavior in the sense of Shilnikov theorem [Chua *et al.*, 1986], and fundamental phenomena such as Andronov–Hopf, saddle-node (tangent), flip (period-doubling), cusp, homoclinic, heteroclinic, and many other kinds of bifurcations [Matsumoto *et al.*, 1986; Bykov, 1998; Medrano-T *et al.*, 2003, 2005, 2006; Algaba *et al.*, 2012]. In this system, domains of periodicity immersed in chaotic regions of 2D parameter space are organized in period-adding cascades with spiral configurations along homoclinic bifurcations [Komuro *et al.*, 1991; Albuquerque & Rech, 2012]. Moreover, the implementation of Chua's circuit is easy and allows to perform experiments whose results present great agreement with computational simulations [Matsumoto *et al.*, 1985; Zhong & Ayrom, 1985; Weldon, 1990; Cruz & Chua, 1992; Kennedy, 1992; Cruz & Chua, 1993; Rodriguez-Vazquez & Delgado-Restituto, 1993; Morgül, 1995; Senani & Gupta, 1998; Elwakil & Kennedy, 2000; Tôrres & Aguirre,

2000; Kiliç *et al.*, 2002; Barboza, 2008; Rocha & Medrano-T, 2009; Trejo-Guerra *et al.*, 2010; Rocha *et al.*, 2010; Banerjee, 2012].

Despite the great number of scientific investigations related to Chua's circuit, there is still a lack of theoretical and experimental investigations related to the *negative side* of its parameter space, where all control parameters are negative. An implementation of the conventional Chua's circuit with negative parameters presents a physical impossibility, since it would need resistances, inductances and/or capacitances with negative values. A negative impedance is an active element that supplies the same power quantity to the electric circuit that would be absorbed by its positive equivalent. A solution for this problem is the use of impedance converters in order to obtain negative values for inductances and/or capacitances [Lahiri & Gupta, 2011; Swamy, 2011]. Another alternative is to rewrite the circuit's equations in order to obtain negative impedance conveyors exclusively associated to resistors [Bartissol & Chua, 1988]. A more interesting option is a versatile and functional inductorless implementation of Chua's circuit based on an electronic analogy [Rocha & Medrano-T, 2009], which allows to explore the whole parameter space with great accuracy and comfortable signal observations, becoming possible to verify a sequence of new experimental attractors. In this context, Chua's circuit with negative parameters can be physically implemented for experimental studies, such that the phenomena investigated in this work can be analyzed both experimentally and theoretically without concerns related to the physical impossibility of impedances with negative values.

For the theoretical point of view, Chua's system presents a homoclinic orbit of a saddle-focus, i.e. a biasymptotic trajectory to a saddle-focus equilibrium point when $t \to \pm\infty$ being a real example where the Shilnikov theorem can be applied. In this case, the theorem states that if the Shilnikov condition[1] is satisfied then there are countable many saddle periodic orbits in a neighborhood of the homoclinic orbit [Shilnikov, 1965]. Chua's system obeys this theorem for positive values of the control parameters, but on the negative side of the parameter space the Shilnikov condition fails [Madan, 1993]. This is just a mathematical possibility that occurs casually in Chua's circuit when the electronic devices are operating in negative values. As a consequence, the Shilnikov theorem, responsible for describing the complexity in Chua's circuit, cannot be applied and the dynamic behavior operates differently than the positive side. Thus a completely new organization emerges in the parameter space never predicted theoretically. While on the positive side, a set of homoclinic bifurcation curves is associated to the change between the behavior of the so-called Rössler-type and double scroll chaotic attractors [Medrano-T *et al.*, 2006], on the negative side, a homoclinic bifurcation curve is the boundary between the symmetric and asymmetric periodic orbits. While on the positive side, sets of periodicity in period-adding are organized in spirals [Komuro *et al.*, 1991; Albuquerque & Rech, 2012], here period-adding in rings are shown and period-adding in continuous sets of periodicity are also observed.

This work reports some theoretical and experimental investigations related to the dynamic behavior of Chua's circuit on the negative side of its parameter space. The diagram and the dynamic model of Chua's circuit are presented in Sec. 2. In Sec. 3, the dynamics of this system is mapped in regions within the parameter space from a stability analysis based on the method of describing functions, which results are numerically corroborated in Sec. 4. An extended numerical study in two-dimensional parameter space reveals an interesting and new scenario of periodic and chaotic dynamics in Sec. 4.3, which cannot be explained under Shilnikov theorem. It is observed that there are Andronov–Hopf and homoclinic bifurcations, cascades of periodicity sets presenting period-adding phenomenon [Kaneko, 1982] and the remarkable presence of the phenomenon known as basin boundary metamorphosis, where the basin boundary of attraction of the attractors changes, under parameter variations, from smooth to fractal up to disappearance [Alligood *et al.*, 1997; Ott, 1993]. The basin boundary metamorphosis and its consequence over the system stability are investigated in Sec. 4.4 from an analysis in the parameter space that requires high computational cost, which consists of a novelty in the study of this phenomenon. Section 5 presents the experimental results obtained from the implementation of the analog Chua's circuit with negative parameters [Rocha & Medrano-T, 2009], which presented a

[1] $|\mathrm{Re}(\mu_2)/\mu_1| < 1$, where μ_1 is the real eigenvalue and μ_2 is one of the complex conjugate eigenvalues of the saddle-focus.

good agreement with theoretical analyses. Finally, the conclusions of this work are presented in Sec. 6.

2. Chua's Circuit

Chua's circuit is an autonomous system composed of a network of linear passive elements, connected to a nonlinear active component. The standard form of Chua's circuit is shown in Fig. 1(a), where the linear resistor R couples a lossless parallel resonant circuit, composed by the inductor L and the capacitor C_2, to a parallel combination between the capacitor C_1 and a nonlinear active power source known as Chua's diode. The dynamics of Chua's circuit can be described by three-coupled first-order nonlinear differential equations

$$\begin{aligned} \dot{v}_1 &= -\frac{v_1 - v_2}{RC_1} - \frac{i_D(v_1)}{C_1} \\ \dot{v}_2 &= \frac{v_1 - v_2}{RC_2} + \frac{i_L}{C_2} \\ \dot{i}_L &= -\frac{v_2}{L}, \end{aligned} \tag{1}$$

where

$$\begin{aligned} i_D(v_1) = m_1 v_1 &+ \frac{1}{2}(m_0 - m_1) \\ &\times (|v_1 + B_p| - |v_1 - B_p|) \end{aligned} \tag{2}$$

is the nonlinear function of Chua's diode, which is characterized by a three segmented piecewise-linear curve with two negative slopes, m_0 and m_1, shown in Fig. 1(b).

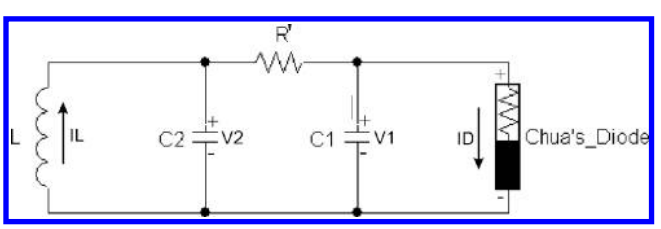

(a)

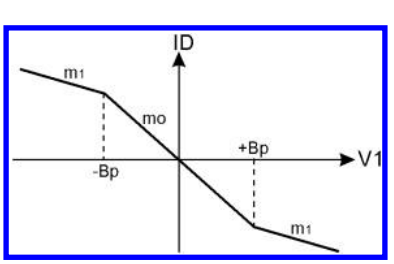

(b)

Fig. 1. Schematic Chua's circuit: (a) Chua's circuit and (b) characteristic of Chua's diode.

An adequate rescheduling of Chua's system allows to group the seven original parameters (R, C_1, C_2, L, m_0, m_1, B_p) in four dimensionless parameters (α, β, a, b), such that it can be rewritten in its dimensionless form as:

$$\begin{aligned} \dot{x} &= \alpha[-x + y + u(x)] \\ \dot{y} &= x - y + z \\ \dot{z} &= -\beta y, \end{aligned} \tag{3}$$

where $\dot{x} = \frac{dx}{d\tau}$, with $\tau = t/RC_2$, and

$$x = \frac{v_1}{B_p}, \quad y = \frac{v_2}{B_p}, \quad z = \frac{Ri_L}{B_p},$$

$$\alpha = \frac{C_2}{C_1}, \quad \beta = \frac{R^2 C_2}{L},$$

$$a = R|m_0|, \quad b = R|m_1|$$

and the scaled nonlinear function associated to Chua's diode is

$$u(x) = bx + \frac{1}{2}(a - b)(|x + 1| - |x - 1|), \tag{4}$$

which divides the system into three regions separated by the planes $x = 1$ and $x = -1$, namely $x < -1$ (region D_-), $|x| \leq 1$ (region D_0), and $x > 1$ (region D_+). The equilibrium points for this system are

$$O = (0, 0, 0) \quad \text{and} \quad \pm P = \left(\pm\frac{a - b}{1 - b}, 0, \mp\frac{a - b}{1 - b}\right).$$

In this work, the parameter region of interest corresponds to the third quadrant of the parameter space ($\alpha < 0$ and $\beta < 0$), the negative side of Chua's parameter space. Note that even here a and b are considered positive, the slopes m_0 and m_1 are negative. Thus, actually, all parameters are negatives in the considered region.

3. Stability Analysis

Since Chua's circuit can be considered a nonlinear feedback system, as illustrated in Fig. 2, its stability can be analyzed by using describing functions. This approach for analysis of nonlinear systems is easily found in several classic books [Ogata, 1970; Slotine & Li, 1991; Khalil, 1996; Glad & Ljung, 2000], consisting of an extension of linear techniques based on the concepts of the frequency response

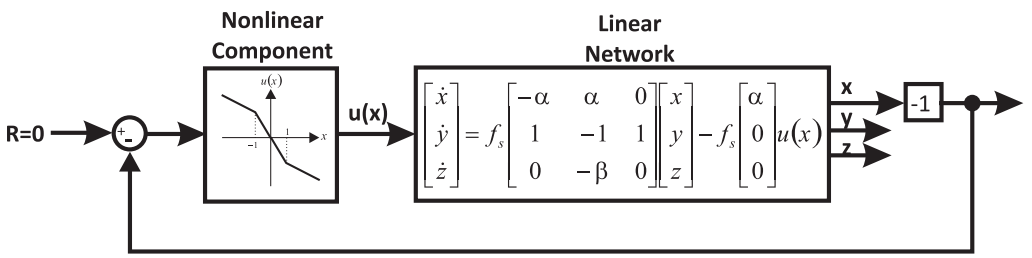

Fig. 2. Chua's circuit as a nonlinear feedback system.

in order to verify effects of certain nonlinearities on a feedback dynamic system. The analysis by describing functions allows to predict stability and the possible existence of limit cycles [Ogata, 1970; Oliveira *et al.*, 2012] and chaotic behavior, which can be interpreted as an interaction between limit cycles and equilibrium points [Genesio & Tesi, 1991; Neymeyr & Seelig, 1991; Genesio & Tesi, 1992; Savacı & Günel, 2006].

The transfer function of the linear part of Chua's circuit between the output x and the input u (see Fig. 2), in series connection with an inverter block, is

$$G(s) = \alpha \frac{s^2 + s + \beta}{s^3 + s^2(1+\alpha) + s\beta + \alpha\beta}, \tag{5}$$

which consists of a low-pass filter. The *frequency response* $G(j\omega)$ is obtained directly from $G(s)$ substituting s by $j\omega$, and can be represented by a closed curve, called *Nyquist diagram*, plotted in the complex plane when the frequency ω is swept from $-\infty$ to $+\infty$.

If a time-invariant nonlinear element as Chua's diode is associated to a linear system with low-pass filter characteristics as $G(s)$, the higher order harmonic components are attenuated such that the fundamental harmonic can be considered the only representative component of the output signal. Thus, a variable gain $N(X)$ known as *describing function* can be defined for this nonlinear element as the relationship between the fundamental component of the output signal and a sinusoidal input excitation $X\sin(\omega t + \theta)$. The describing function of the three-segmented piecewise-linear curve $u(x)$ of Chua's diode is

$$N(X) = \begin{cases} -a & \text{for } |X| < 1, \\ -b - \dfrac{a-b}{\pi}(\theta + \sin\theta) & \text{for } |X| \geq 1, \end{cases} \tag{6}$$

where

$$\theta = 2\arcsin\left(\frac{1}{X}\right), \tag{7}$$

for $\theta \in [0, \pi]$. Thus, the Nyquist's criterion can be extended to analyze the stability of Chua's circuit. This feedback system presents limit cycles if its characteristic equation

$$1 + N(X)G(j\omega) = 0 \tag{8}$$

is satisfied, which means that the Nyquist's diagram $G(j\omega)$ must intercept the geometric locus $-1/N(X)$ at some point of the complex plane. Considering that $G(j\omega)$ encircles n_c times clockwise and n_u times counterclockwise $-1/N(X)$, the origin O is stable only if $n_c - n_u = n_p$, where n_p is the number of poles of $G(s)$ in the right-half complex plane. As can be verified by Ruth–Hurwitz criterion, this $G(s)$ has two poles with positive real parts for $\alpha < 0$ and $\beta < 0$ ($n_p = 2$), such that the equilibrium point O is stable for this feedback system only if $n_c - n_u = 2$. Otherwise, Chua's circuit with negative parameters is unstable.

Since the geometric locus $-1/N(X)$ of Chua's diode corresponds to a line segment over the real axis in the complex plane that begins at $1/a$ and tends to $1/b$ when $X \to \infty$, it can be only intercepted by the Nyquist's diagram $G(j\omega)$ when $\mathrm{Im}[G(j\omega)] = 0$, such that the possible interception points p_i and their associated frequencies ω_i are shown in Table 1, where $\gamma = (1+\alpha)/2$.

Some considerations can be highlighted about these interception points. Although the oscillation frequency $\omega_0 = \pm\infty$, the amplitude of the limit cycle related to p_0 is null, which is expected since $G(s)$ is a low-pass filter, such that this interception point corresponds to the equilibrium point O. Since the amplitude is different to zero for an oscillation frequency $\omega_1 = 0$, the limit cycle related to the interception point p_1 corresponds to the equilibrium points $\pm P$. The frequency ω_3 is always complex for

Table 1. Solutions of limit cycles and equilibrium points.

i	ω_i	$p_i \doteq G(j\omega_i)$	Invariant Set
0	$\pm\infty$	0	O
1	0	1	$\pm P$
2	$\pm\sqrt{\beta-\gamma+\sqrt{\gamma^2-\beta}}$	$\dfrac{\alpha}{\gamma-\sqrt{\gamma^2-\beta}}$	limit cycle
3	$\pm\sqrt{\beta-\gamma-\sqrt{\gamma^2-\beta}}$	$\dfrac{\alpha}{\gamma+\sqrt{\gamma^2-\beta}}$	limit cycle

$\alpha < 0$ and $\beta < 0$, such that the interception point p_3 does not exist on the negative side of the parameter space of Chua's circuit. For $\alpha > \beta$, the frequency ω_2 is complex and the interception point p_2 does not exist. Therefore, Nyquist's diagram crosses the real axis twice (in p_0 and p_1) and $-1/N(X)$ can only be encircled one time by $G(j\omega)$ ($n_c - n_u = 1$), as shown in Fig. 3. According to Nyquist's criterion, Chua's system is always unstable in this region. When $\alpha < \beta$, the frequency ω_2 is real and the Nyquist's diagram crosses the real axis three times. Thus, $G(j\omega)$ can encircle twice $-1/N(X)$ as can be seen in Fig. 4, and the dynamics of Chua's circuit can evolve from a fixed equilibrium point to a route to chaos.

It is necessary to analyze the describing function around the interception point in order to verify its stability. Considering Fig. 4(a) as example, the Nyquist's diagram (black curve) intercepts the negative inverse of the describing function (red curve) at p_1 and p_2 for $a < 1/p_2$ and $b > 1$, which configures the existence of an equilibrium point (p_1) and a limit cycle (p_2). The right side of p_2 is an unstable region since it is not encircled twice by the Nyquist diagram, so that the amplitude X of this limit cycle increases and the operation point moves over $-1/N(X)$ from right to left in direction to p_2. On the other side of p_2, the yellow region is encircled clockwise twice and the origin O is stable ($n_c - n_u = 2$), such that X decreases and the operation point moves in the direction of p_2. Therefore, p_2 is a stable limit cycle with frequency ω_2. On the other hand, p_1 is an unstable equilibrium point since X decreases and moves the operation point to p_2 in the stable yellow region, while X converges to infinite in the unstable region to the left of p_1, which is only encircled once by Nyquist's diagram ($n_c - n_u = 1$). Due to the proximity between p_1 and p_2, the unstable equilibrium point can interact with the stable limit cycle, promoting a chaotic behavior [Genesio & Tesi, 1991, 1992]. Thus, Fig. 4(a) indicates that it is possible to observe periodic, chaotic, and divergent orbits for $\alpha < \beta$, $a < 1/p_2$, and $b > 1$. This same analysis can be applied in order to verify the stability of the interception points and to identify possible dynamic behavior of Chua's circuit for each situation that is described in Figs. 4(b) to 4(i).

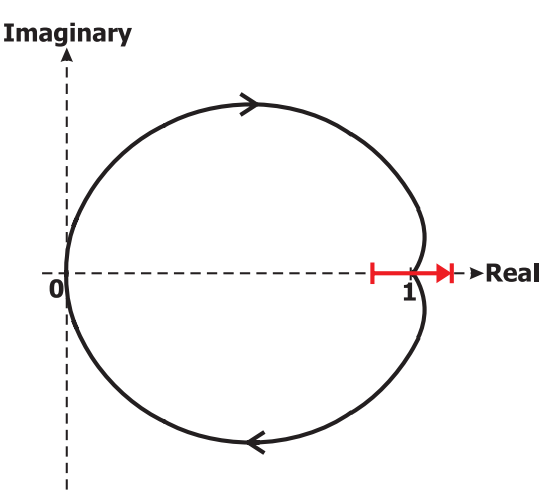

Fig. 3. Nyquist's diagram for $\alpha > \beta$. Since the geometric locus $-1/N(X)$ (red curve) cannot be encircled by $G(j\omega)$ (black curve) twice, the system is always unstable in this situation.

The stability analysis of Chua's circuit in the region $\alpha < \beta$ is summarized in the parameter space $b \times a$ as shown in Fig. 5(a), which follows the distribution of the pictures presented in Fig. 4. It is noted that a chaotic behavior in Chua's circuit with negative parameters can only be obtained if $a > 1$ and $b < 1$ or vice versa. This map $b \times a$ still shows that the region $\alpha < \beta < 0$ can be divided into two distinct areas, since the route to chaos begins when the smallest slope of $u(x)$ becomes equal to $1/p_2$ or

$$\beta = \alpha \min(a, b)[1 + \alpha(1 - \min(a, b))], \qquad (9)$$

which establishes the points where a Andronov–Hopf bifurcation occurs. From this stability analysis, Chua's circuit dynamics can be mapped in the third quadrant of the parameter space $\beta \times \alpha$ for fixed slopes, which is presented in Figs. 5(b) and 5(c). The only difference between these maps $\beta \times \alpha$ is that the stable equilibrium point for $a > 1$ and $b < 1$ is $\pm P$, while the same region for $a < 1$ and $b > 1$ corresponds to an unstable limit cycle.

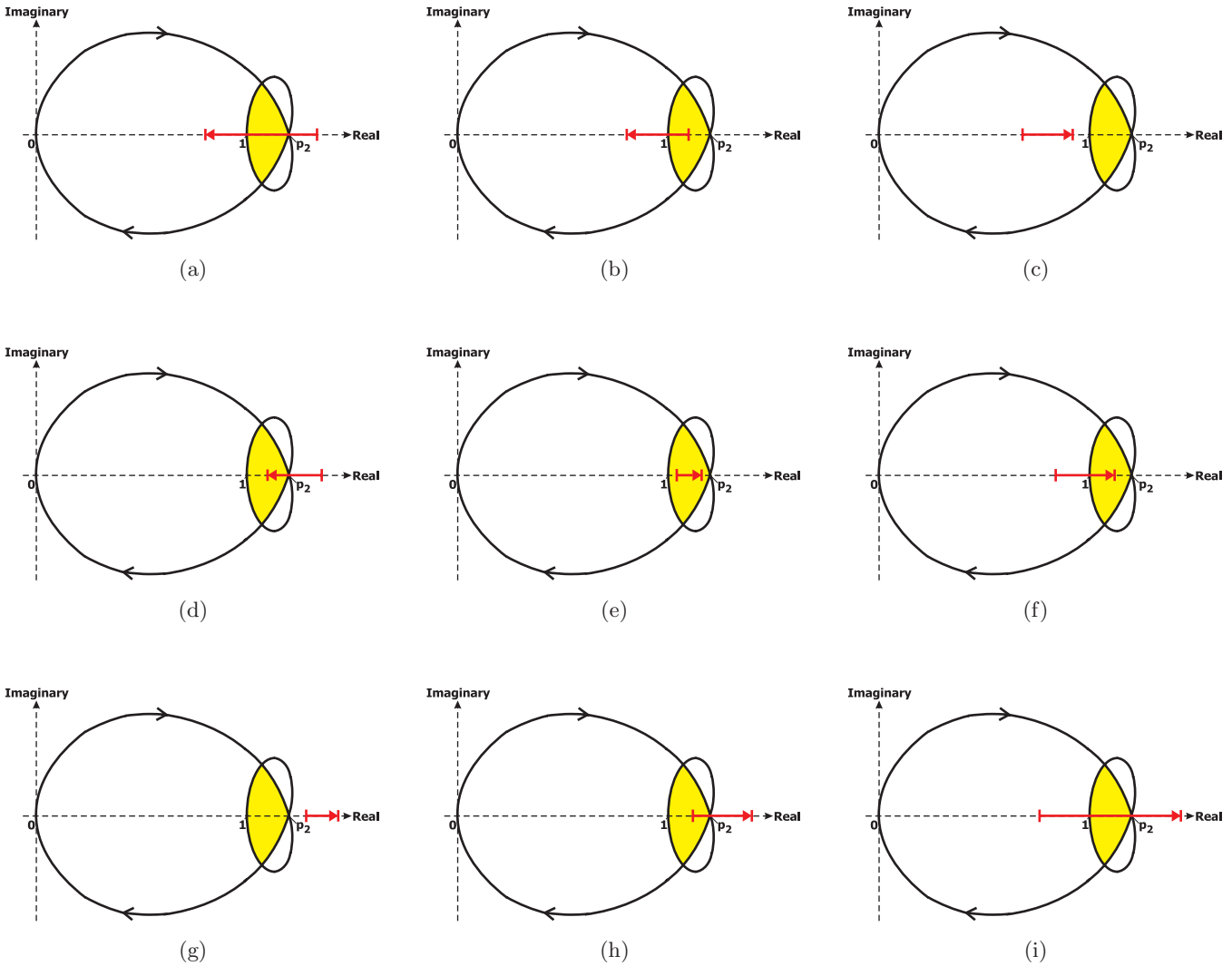

Fig. 4. Nyquist's diagrams for $\alpha < \beta$. (a) $a < 1/p_2$ and $b > 1$: $-1/N(X)$ intercepts $G(j\omega)$ at two points that respectively correspond to an unstable equilibrium point and a stable limit cycle, which can interact and produce a periodic or chaotic dynamics whose fundamental frequency is ω_2 or become unstable according to initial conditions; (b) $1/p_2 < a < 1$ and $b > 1$: $-1/N(X)$ intercepts $G(j\omega)$ at a point that corresponds to an unstable limit cycle, such that the dynamics converges to the stable origin O or becomes unstable according to initial conditions; (c) $a > 1$ and $b > 1$: $-1/N(X)$ is encircled by $G(j\omega)$ only one time such that the dynamics is unstable; (d) $a < 1/p_2$ and $1/p_2 < b < 1$: $-1/N(X)$ intercepts $G(j\omega)$ at a point that corresponds to a stable limit cycle whose frequency is ω_2; (e) $1/p_2 < a < 1$ and $1/p_2 < b < 1$: $-1/N(X)$ is completely encircled by $G(j\omega)$ twice such that the dynamics converges to the stable origin O; (f) $a > 1$ and $1/p_2 < b < 1$: $-1/N(X)$ intercepts $G(j\omega)$ at a point that corresponds to a stable equilibrium point $\pm P$ for which the dynamics converges; (g) $a < 1/p_2$ and $b < 1/p_2$: $-1/N(X)$ is not encircled by $G(j\omega)$ and the dynamics is unstable; (h) $1/p_2 < a < 1$ and $b < 1/p_2$: $-1/N(X)$ intercepts $G(j\omega)$ at a point that corresponds to an unstable limit cycle, such that the dynamics can converge to the stable origin O or become unstable according to initial conditions; (i) $a > 1$ and $b < 1/p_2$: $-1/N(X)$ intercepts $G(j\omega)$ at two points that respectively correspond to a stable equilibrium point and an unstable limit cycle, which can interact and produce a periodic or chaotic dynamics whose fundamental frequency is ω_2 as well as become unstable according to initial conditions.

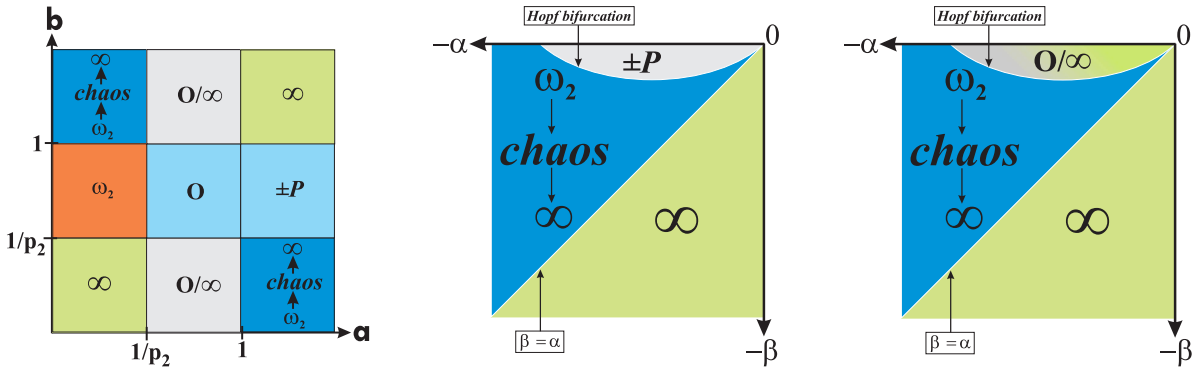

(a) (b) (c)

Fig. 5. Mapping sketch for parameter spaces from stability analysis: (a) $b \times a$ for $\alpha < \beta$, (b) $\beta \times \alpha$ for $a > 1$ and $b < 1$ and (c) $\beta \times \alpha$ for $a < 1$ and $b > 1$. O or $\pm P$ (gray) = stable equilibrium point; ω_2 (brown) = stable limit cycle with frequency ω_2; O/∞ (gray/green) = unstable limit cycle; $\omega_2 \to chaos \to \infty$ (dark blue) = route to chaos; ∞ (green) = unstable dynamics.

4. Numerical Simulations

One of the most outstanding characteristics of Chua's circuit is the presence of chaotic and periodic behaviors due to Shilnikov theorem, i.e. there are Cantor sets close to a saddle-focus homoclinic orbit under the Shilnikov condition [Chua *et al.*, 1986; Komuro *et al.*, 1991; Guckenheimer & Holmes, 1983]. For these conditions, it is well known that this system presents continuous spiral sets of periodicity along homoclinic bifurcation curves immersed in a chaotic sea [Gaspard *et al.*, 1984; Komuro *et al.*, 1991; Medrano-T & Caldas, 2010; Albuquerque & Rech, 2012; Hoff *et al.*, 2014]. Nevertheless, on the negative side of Chua's circuit, the Shilnikov condition is not satisfied and domains of periodicity are organized completely different from the *positive side* (parameter space with $\alpha > 0$ and $\beta > 0$). Hereafter, we present this new scenario for $a = 8/7$ and $b = 5/7$. The results are in complete agreement of the theoretical analysis depicted in Fig. 5(b).

4.1. *Global view*

In Fig. 6, periodic and chaotic behaviors are identified according to the maximum Lyapunov exponent λ, excluding the null exponent. In the region of periodic attractor ($\lambda < 0$), λ decreases from white to brown, and in the region of chaotic attractor ($\lambda > 0$), the chaoticity grows as λ increases from white to blue. Stable equilibrium points [namely, $\pm P = (\pm 1.5, 0, \mp 1.5)$] are in the gray region identified by computing its eigenvalues (μ_1, $\mathrm{Re}(\mu_{2,3}) < 0$), while trajectories with distance greater than 10 from the origin are considered divergent (green region). The black line in the boundary between the equilibrium and periodic attractor regions denotes an Andronov–Hopf bifurcation curve which, according to Eq. (9), is given by

$$\beta = \frac{5}{7}\alpha\left(1 + \frac{2}{7}\alpha\right), \tag{10}$$

and the dashed line is a homoclinic bifurcation curve determined by the method presented in [Medrano-T *et al.*, 2003]. The dot dashed line ($\beta = \alpha$) indicates the regions where attractors are expected as theoretically determined in Sec. 3 [see Fig. 5(b)]. It is further explored in a new scenario contained in Fig. 6.

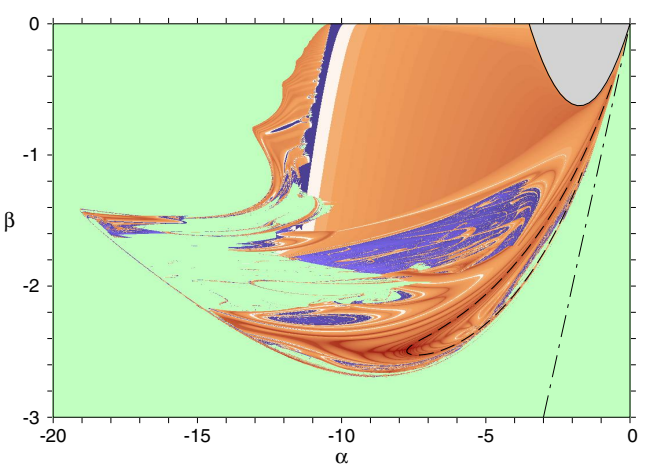

Fig. 6. Attractors in the $\beta \times \alpha$ space: equilibrium (gray), periodic (brown), chaotic (blue), and infinity (green). The continuous and dashed lines correspond to the Andronov–Hopf and homoclinic bifurcations, respectively. And the dot dashed line ($\beta = \alpha$) splits the attractor and the divergent regions.

4.2. *Homoclinic bifurcation*

Since the Shilnikov condition is not satisfied, there are no chaotic sets close to the homoclinic orbit. Thus a continuous set of periodicity is formed around the homoclinic bifurcation curve as shown in Fig. 7(a). Note that curves with dark brown color are densely accumulating along the homoclinic bifurcation curve. These curves represent periodic orbits with *high stability*, where trajectories are strongly attracted to periodic orbits when compared with neighboring orbits in the parameter space, i.e. λ is a local minimum. A magnification sequence of the maximum Lyapunov exponent around an accumulation point at $\beta = -2.35$ is shown in Figs. 7(b) to 7(d). A homoclinic orbit is formed for $(\alpha, \beta) \approx (-6.769, -2.350)$.

For a continuous change of a control parameter, two homoclinic orbits are formed due to the collision between two anti-symmetric periodic attractors at the origin, where the equilibrium saddle-focus O is. These orbits merge yielding a symmetric periodic attractor. This process can be viewed in Figs. 7(e) to 7(g) where $\beta = -2.5$ is fixed. In Fig. 7(e) the two anti-symmetric periodic attractors are shown for $\alpha = -9.0$ that collide in Fig. 7(f), where the two homoclinic orbits are shown for $\alpha \approx -7.737$, and in Fig. 7(g) is the resultant symmetric periodic attractor for $\alpha = -7.5$. The same process is observed from Figs. 7(i) to 7(g). The place in the parameter space relative to these processes is displayed in Fig. 7(a) by + symbols.

4.3. *Period-adding in sets of periodicity*

Period-adding [Kaneko, 1982] is a phenomenon observed in the parameter space, where, in a cascade of periodic orbits, the revolution difference between two consecutive periodic attractors is given

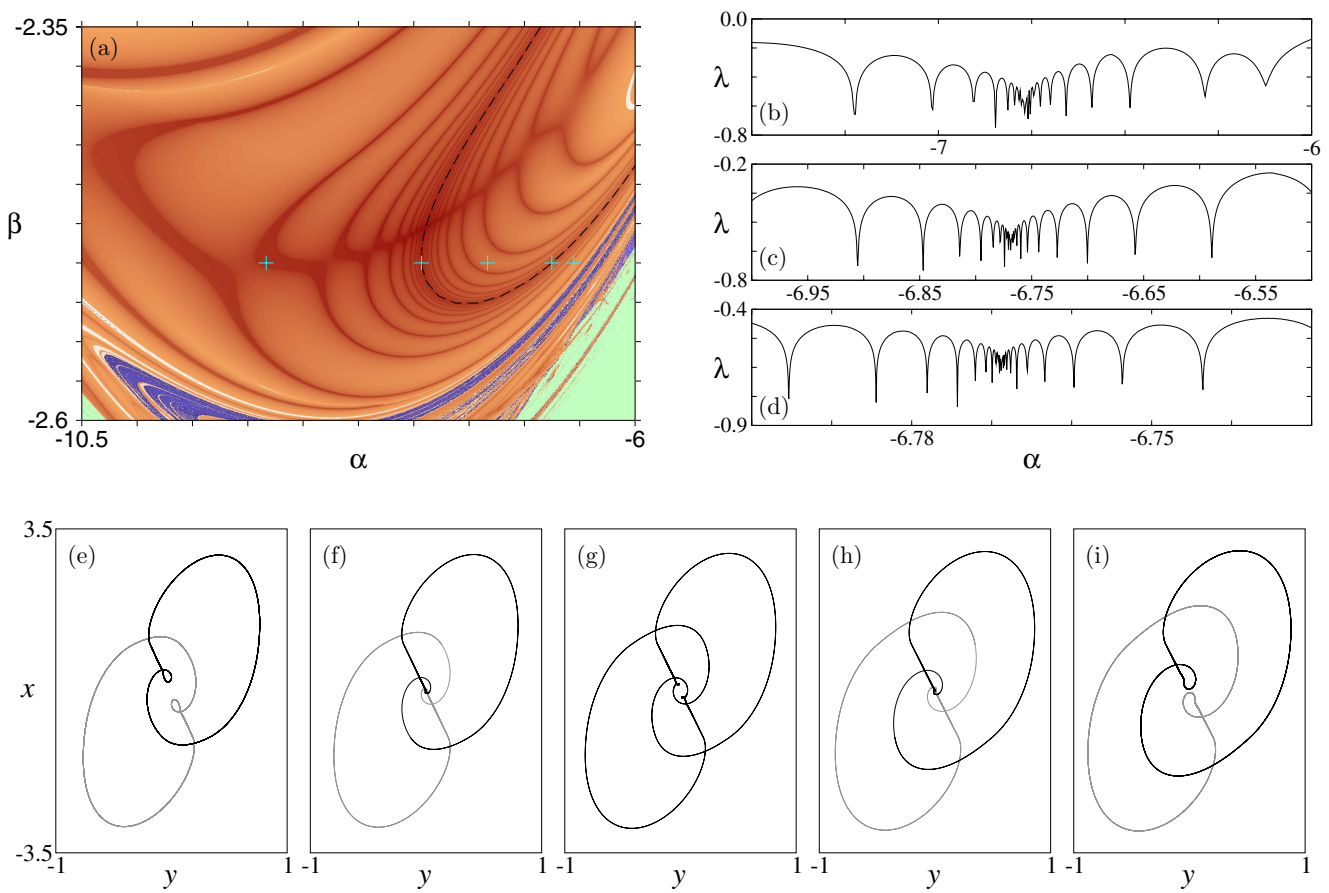

Fig. 7. (a) Accumulation of high stability regions (dark brown sets) in a homoclinic bifurcation curve (dashed line). (b)–(d) Sequences of the maximum Lyapunov exponent (λ) with successive magnifications for $\beta = -2.35$. (e)–(i) Stable periodic orbits for $\beta = -2.5$ fixed and (e) $\alpha = -9.0$, (g) $\alpha = -7.2$, and (i) $\alpha = -6.5$, and homoclinic orbits for (f) $\alpha \approx -7.737$ and (h) $\alpha \approx -6.677$. In gray is the anti-symmetric invariant set. The local of these sets in the parameter space are indicated by + symbols in (a).

by a constant ρ. The cascade can appear in continuous or discrete sets of periodicity and have been recently the subject of several works in different areas [Bonatto & Gallas, 2007; da Silva *et al.*, 2009; de Souza *et al.*, 2012; Medeiros *et al.*, 2013; So *et al.*, 2014; Rech, 2013; Stegemann & Rech, 2014].

4.3.1. *Continuous sets*

A continuous domain of periodicity between divergent and chaotic regions is shown in Fig. 8(a). The parameter λ along the dashed line is evaluated in Fig. 8(b) making explicit the self-similarity of this structure. Four parameters in consecutive similar regions of this figure [and in Fig. 8(a)] are marked by + of which the respective periodic attractors are shown from Figs. 8(c) to 8(f), respectively. Note that the number of revolutions follows the sequence $5 \to 6 \to 7 \to 8$ when the parameters increase characterizing the period-adding phenomenon with constant $\rho = 1$. This period-adding in continuous sets was never observed on the positive side of the parameter space.

4.3.2. *Discrete sets*

We call period-adding in discrete sets of periodicity the cascade composed by domain of periodicity interspersed with domains of irregular behavior. This case was previously reported for Chua's system with positive parameters in [Komuro *et al.*, 1991; Albuquerque & Rech, 2012].

In Figs. 9(a) and 9(b), it is observed that an accumulation of a sequence of structures is called shrimps in an horizon [Bonatto & Gallas, 2007; Medeiros *et al.*, 2013], where the numbers refer to

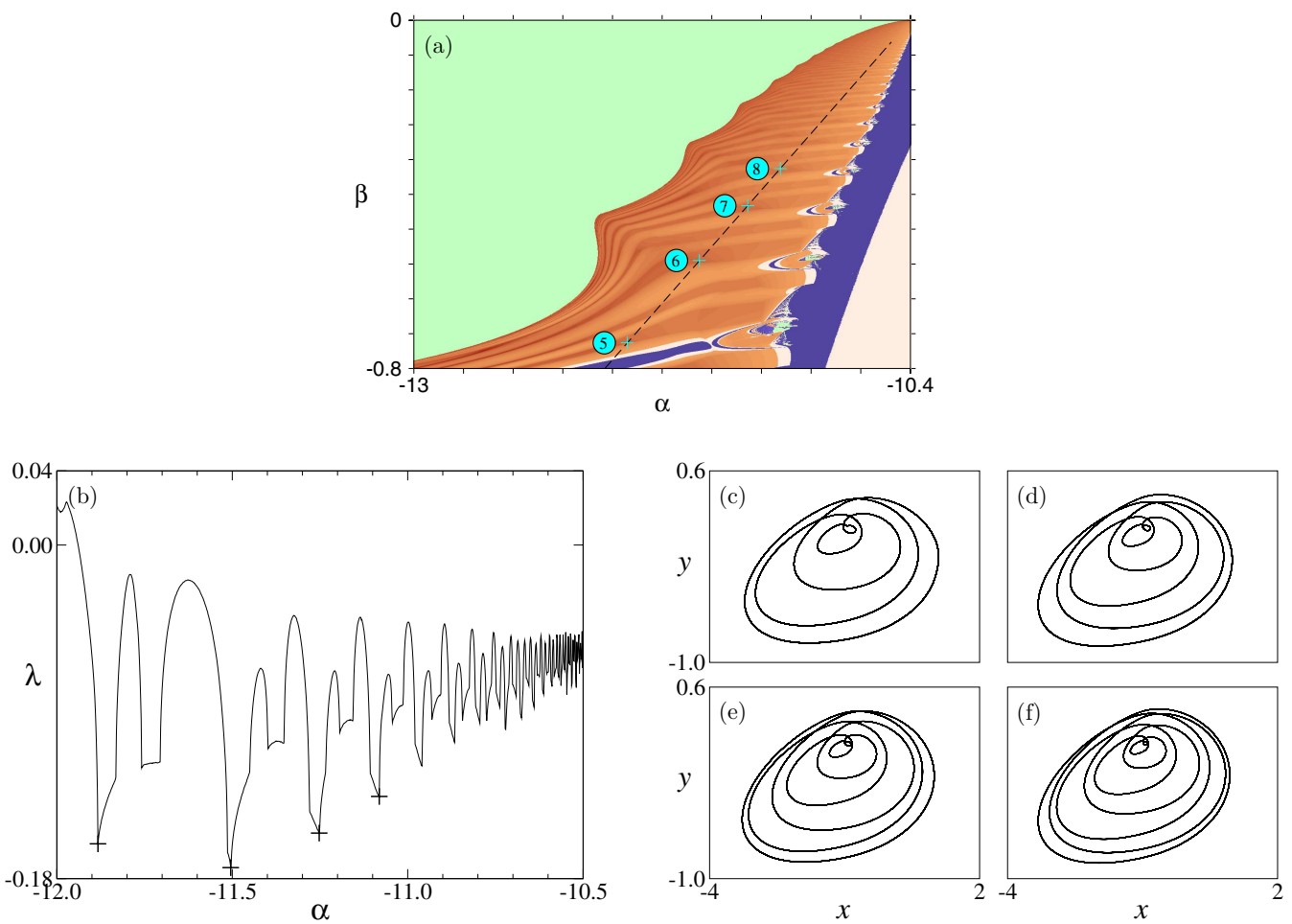

Fig. 8. Period-adding phenomenon ($5 \to 6 \to 7 \to 8$) in continuous domain with periodic behavior. (a) Detail of Fig. 6. (b) Maximum Lyapunov exponent along the black dashed line in (a). Periodic orbits in period-adding characterized by $\rho = 1$: (c) 5-period $(\alpha, \beta) = (-11.850, -0.725)$, (d) 6-period $(-11.500, -0.550)$, (e) 7-period $(-11.250, -0.425)$ and (f) 8-period $(-11.090, -0.345)$.

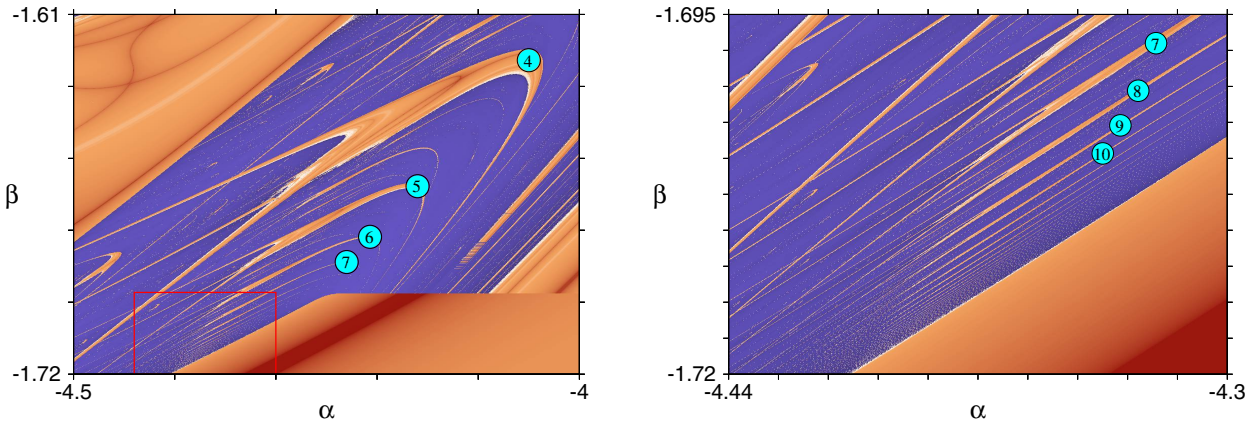

(a) (b)

Fig. 9. Period-adding between chaotic regions with $\rho = 1$.

the main period [4 → 5 → 6 → 7 in (a) and 7 → 8 → 9 → 10 in (b)] that characterize such structures and reveal $\rho = 1$ between two consecutive shrimps in this sequence.

This period-adding composed by accumulations of shrimps in horizons, shown in Fig. 9, is also present on the positive side of the parameter space. But, while the positive side presents period-adding associated to shrimps in spiral structures accumulating in the homoclinic bifurcation point [Gaspard *et al.*, 1984; Komuro *et al.*, 1991; Albuquerque & Rech, 2012], the period-adding on the negative side is observed in structures with ring-like shape (Fig. 10). The accumulation is at a point in the center of the rings since, in this direction, the period increases while the rings decrease in size. The period-adding (24 → 28 → 32) as shown in Fig. 10 is characterized by $\rho = 4$.

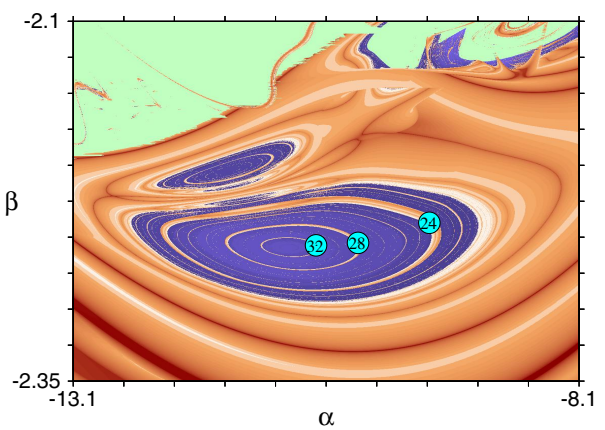

Fig. 10. Period-adding in ring structure with $\rho = 4$.

4.4. *Basin of attraction metamorphoses*

Contrary to the positive side of parameter space, where the boundary between the divergent and attractive regions is well defined, this boundary on the negative side is complex and irregular as shown in Fig. 6. Here, we investigate the role of the basin of attractions of the divergent and attractive regions. The attracting equilibrium, periodic, and chaotic orbits are called generically as attractor, while the infinite attractor refers to the attractor at the infinite.

To introduce the problem, in Figs. 11(a)–11(d), a sequence is considered of four basins of attractions for decreasing values of β. Initial conditions that converge to the attractor are colored in black, and correspond to the basin of attraction of attractor B_A. Similarly the green region corresponds to the basin of attraction of the infinite attractor B_I. Trajectories with distance $d < 10$ from the origin, after an evolution of $\Delta t = 2 \times 10^3$, are considered in the attractor, otherwise, in the infinite attractor. It is clear that in the sequence of Figs. 11(a)–11(d) the basin B_I grows gaining space of basin B_A such that the basin boundary changes from smooth to fractal. This phenomenon, observed since [Guckenheimer & Holmes, 1983; Moon & Li, 1985], is called *basin boundary metamorphosis* [Grebogi *et al.*, 1987; Alligood *et al.*, 1997; Ott, 1993; Robert *et al.*, 2000] and plays an important role in the system stability in the sense that disturbances introduced by intrinsic noise can promote changes in the trajectory.

In the positive region of the parameter space, the famous double scroll attractor dies abruptly

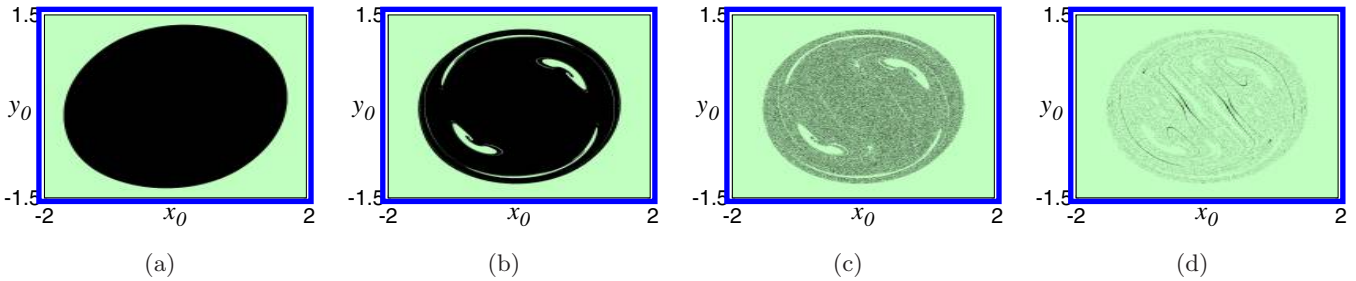

Fig. 11. Basin of attraction metamorphosis. Initial conditions on the black (green) region converge to the attractor (infinite attractor). It is fixed in all pictures $z_0 = 0.0$ and $\alpha = -4.0$. (a) $\beta = -1.8700$, (b) $\beta = -2.0000$, (c) $\beta = -2.0070$ and (d) $\beta = -2.0086$.

when it collides with a periodic saddle, defining a boundary between the sets B_A and B_I [Matsumoto *et al.*, 1985, 1986; Chua *et al.*, 1986]. According to Fig. 11, the attractors in the negative region of the parameter space can lose stability due to the metamorphosis of its basin. It is caused by the presence of a saddle periodic orbit in the basin boundary. Actually, the basin boundary is the stable manifold

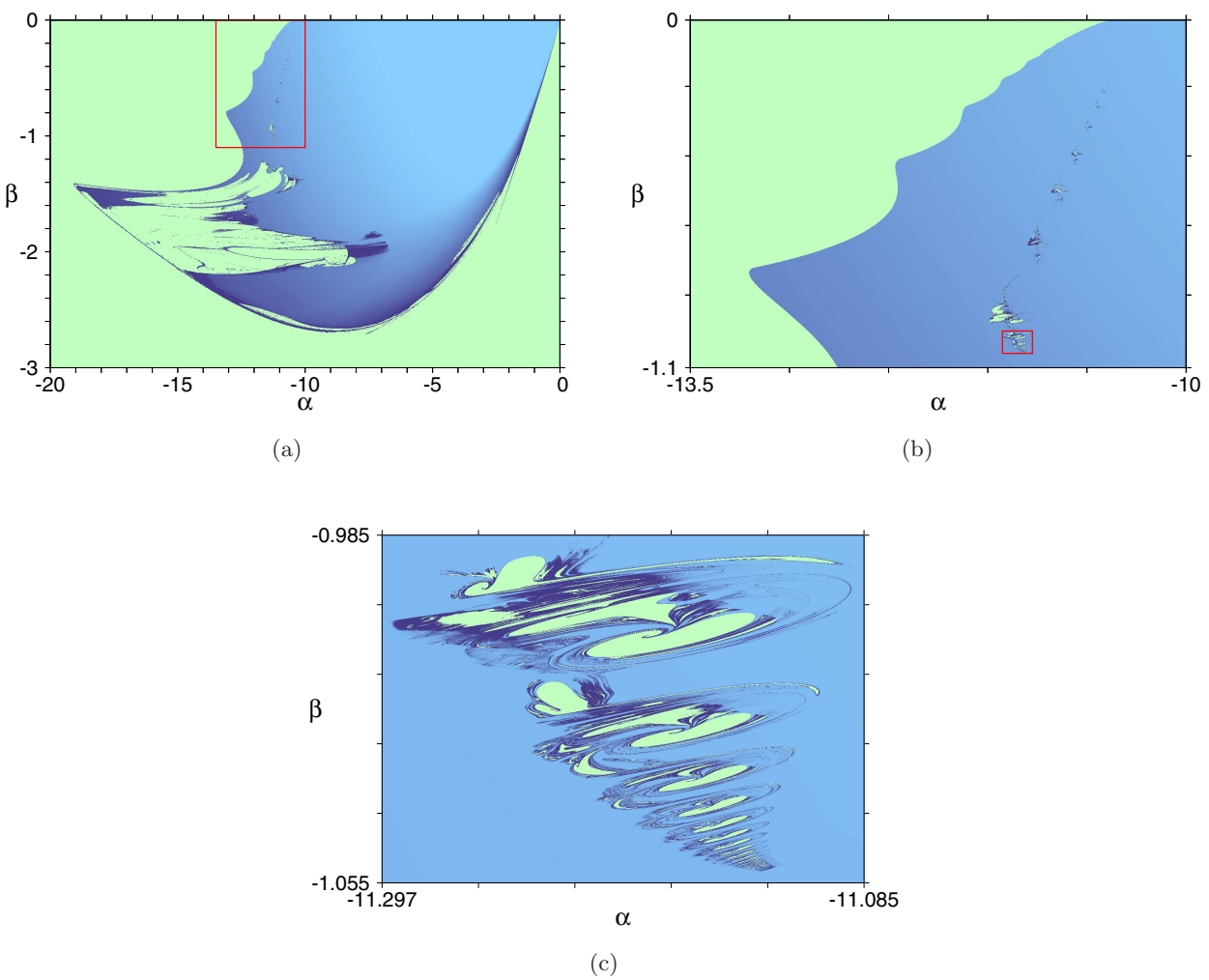

Fig. 12. Stability of Chua's system in the parameter space. The system is unstable in the green region. Its stability grows from dark blue to light blue, where hue variations indicate the presence of fractal basin boundary and metamorphosis phenomenon. (a) General view of the stable region, (b) smooth boundary between the stable and unstable regions and (c) complex self-similarity in the system stability. Red boxes indicate the magnified regions.

of this saddle. When a control parameter changes continuously, the stable and unstable manifolds of the saddle collide (*homoclinic tangency*) a Cantor set emerging responsible for the fractal feature of the boundary. This process is known as *smooth-fractal* metamorphosis [see Figs. 11(a) and 11(b)]. When the control parameter is again varied, the stable manifold of another saddle periodic orbit is subjected to a new homoclinic tangency, causing a *fractal–fractal* boundary metamorphosis with the basin B_A decreasing in size. This is the mechanism that conduces the basin in Figs. 11(b) and 11(c) and in Figs. 11(c) and 11(d). Thus, the presence of several periodic orbits of saddle type embedded in a chaotic set causes a series of changes in the basin boundary whenever a homoclinic tangency occurs until the basin B_A disappears altogether.

A broader investigation can be performed in order to examine the probability of a trajectory to achieve the attractor from the considered initial conditions set. Let us consider $S = n_A/n_0$, where n_0 is the total number of initial conditions and n_A is the number of initial conditions in B_A, as a kind of stability measurement in the sense that the system dynamics can asymptotically converge in probability to an attractor from a random set of initial conditions, this analysis is presented in Fig. 12 for a homogeneous $\beta \times \alpha$ ($10^3 \times 10^3$) for $n_0 = 10^4$. Since this system is dynamically symmetric, the initial conditions are uniformly distributed in the range $x_0 \in [-2.0, 2.0]$ and $y_0 \in [0, 0.75]$, with $z_0 = 0.1$ in order to avoid trajectories with slow velocity. The set for which all trajectories converge to the infinite attractor ($S = 0.0$) corresponds to the green region, while the set for which some trajectories achieve an attractor corresponds to the blue region. The basin of attraction of the attractor corresponding to the light blue region ($S \in [1.0, 0.5]$) is weakly fractal or completely smooth as in Figs. 11(a) and 11(b). The color changes from light to dark blue as the fractality increases ($S \in (0.0, 0.5]$) as shown in Figs. 11(c) and 11(d), characterizing regions with intense action of the basin metamorphosis. Complex structures in a self-similar distribution are identified in the blue region and can be seen in Fig. 12(b), whose remarkable complexity and self-similarity are highlighted in Fig. 12(c). In this region, the Chua's circuit can be considered highly unstable since the inherent noise of experiments changes continuously the initial conditions and the parameters in such a way that the trajectories achieve the basin of the infinite attractor, as observed experimentally in Sec. 5.

5. Experimental Results

The experimental investigation is performed using the analogous Chua's circuit proposed in [Rocha & Medrano-T, 2009], which allows to observe a large variety of attractors. The analogous Chua's circuit used in the experiments is shown in Fig. 13, and its design is based on the methodology described in [Rocha *et al.*, 2006] such that the amplitudes of all output signals are restricted to ± 2 V considering $\alpha = -4.00$, $\beta = -2.00$, $a = -8/7$, and $b = -5/7$. The linear network of conventional Chua's circuit is emulated by analog-inverting weighted integrators with the four op-amps TL074, while the three-segmented piecewise-linear curve of Chua's nonlinearity is synthesized by using an inverter amplifier TL071 with switched gain by polarized diodes. The dynamics of this circuit is determined by the three capacitors C, which are 4.7 nF for this implementation. Analog multipliers AD633 are included in x-cell and z-cell in order to allow explicit variations of the dimensionless parameters α and β, which are represented by external DC voltage levels that can be easily varied by using an external device.

The experimental apparatus for data acquisition and signal processing is presented in Fig. 14. The electronic signals generated by the analogous Chua's circuit are captured using a data acquisition device (DAQ) NI USB-6009 and processed in a computer using the LabVIEW environment, a software widely used for data acquisition, prototyping and testing, which contains a comprehensive set of tools for acquiring, analyzing, displaying, and storing data. This DAQ also performs the generation of two DC signals to adjust the dimensionless parameters α and β of Chua's circuit. The following aspects of the time series are analyzed in order to perform the experimental characterization of the dynamic behavior of the system: time waveforms, phase portraits, frequency spectra, Poincaré sections, and bifurcation diagram. The real-time analysis of the acquired data are performed using LabVIEW codes described in [Rocha *et al.*, 2010].

A series of experimental phase portraits is presented in Fig. 15 for $-4.50 \leq \alpha \leq -1.50$ and $-2.30 \leq \beta \leq -1.04$. These attractors are difficult to detect during experimental procedures because

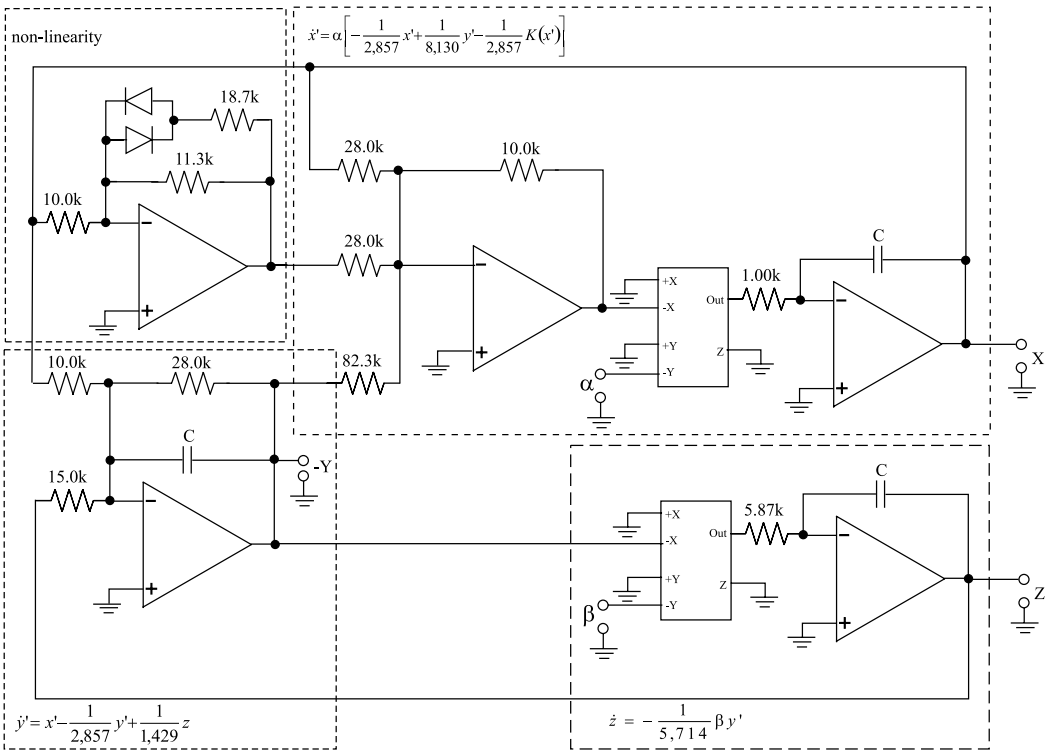

Fig. 13. Analog Chua's circuit.

of problems previously discussed in Sec. 4.4. Focusing the analysis on $\alpha = -4.00$, the attractor evolves from 1-period ($\beta = -1.38$) to 2-period limit cycle ($\beta = -1.41$) as part of the route to chaos via a cascade of period-doubling bifurcation, reaching the first chaotic attractor at $\beta = -1.55$. From a 2-period orbit at $\beta = -1.65$, the dynamics crosses several periodic windows a second time to attain a chaotic attractor at $\beta = -1.78$, returning to a single revolution orbit at $\beta = -2.04$. Due to the odd symmetry of the system $[g(-x) = -g(x)]$, two attractors coexist in this range of β such that, according to initial conditions, the dynamics can converge to an attractor that oscillates around the equilibrium $+P$, crossing the regions D_+ and D_0, or to a symmetric attractor oscillating around the equilibrium $-P$, visiting the regions D_- and D_0. This fact is similar to Rössler-type attractor in the positive parameter space, where there also exists a coexistence of two anti-symmetrical attractors [Rocha & Medrano-T, 2009]. In Fig. 15 for $\alpha = -4.00$ and $\beta = -2.12$ to -2.15, as a result of a collision between attractors, two anti-symmetric attractors merge in a single symmetric attractor that visit all regions D_-, D_0, and D_+.

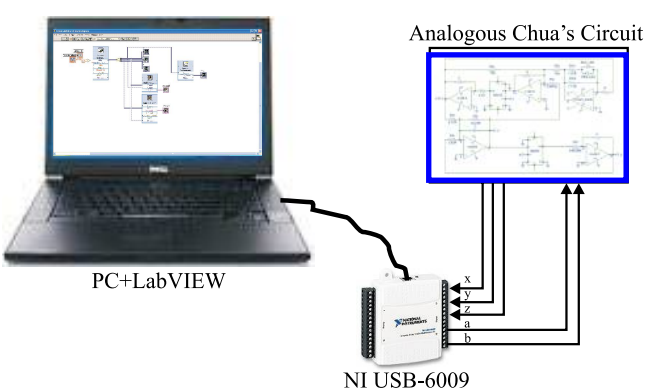

Fig. 14. Experimental apparatus for data acquisition.

This evolution of attractor in the negative space parameter can also be observed in the experimental bifurcation diagram $z \times \beta$ presented in Fig. 16 as well as in two numerically simulated bifurcation diagrams $x \times \beta$ shown in Fig. 17 corresponding to attractors that oscillate around $-P$ in black and around $+P$ in gray. This analysis performed for $\alpha = -4.00$ can be expanded for other sequences of attractors shown in Fig. 15, where it is also possible to observe the existence of asymmetric chaotic attractors that visit all regions. Possible discrepancies between experimental and simulation results can be explained by approximations and uncertainties involving the values of the components utilized in the implementation, which does not exactly

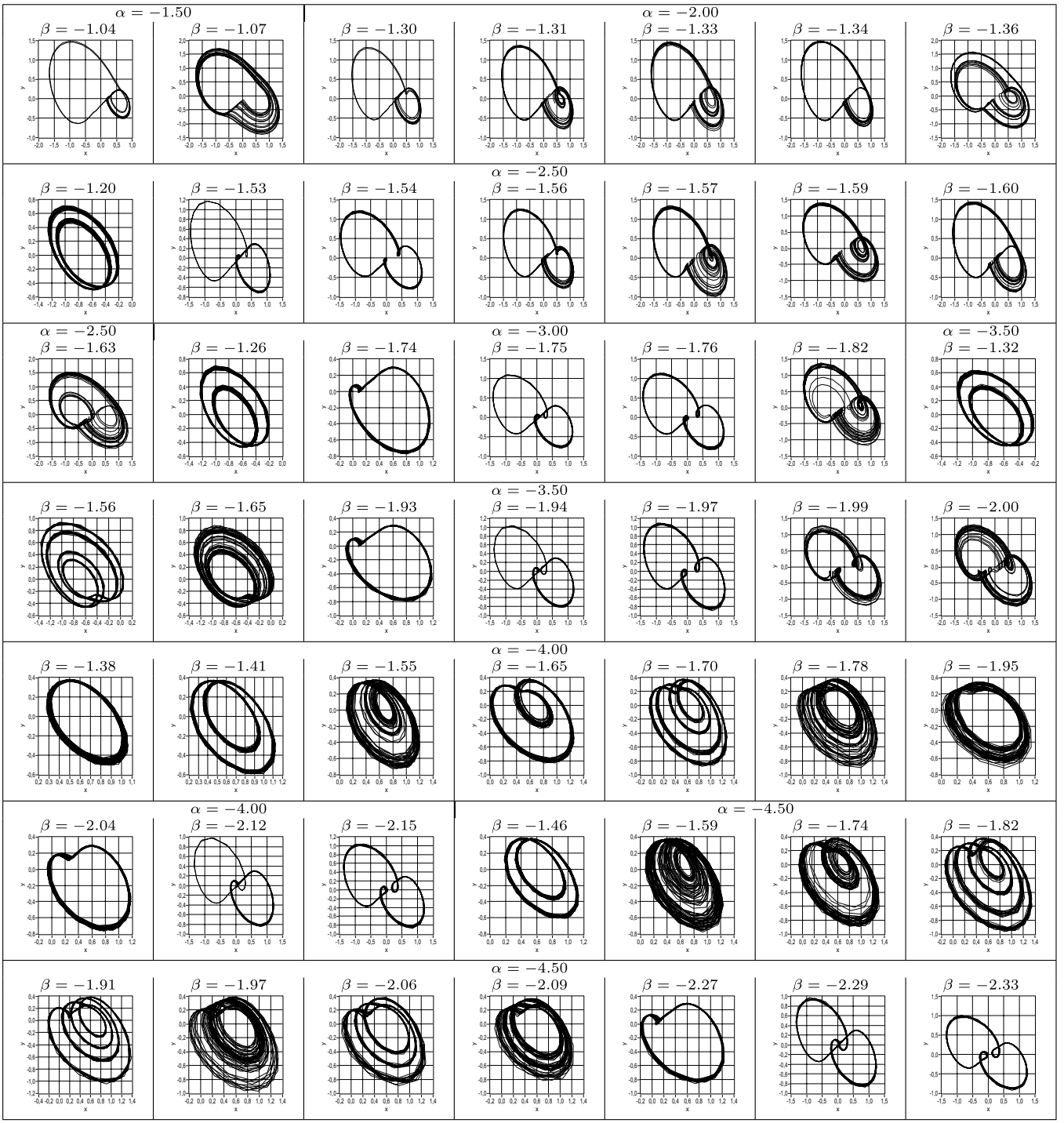

Fig. 15. Experimental attractor projections $y \times x$.

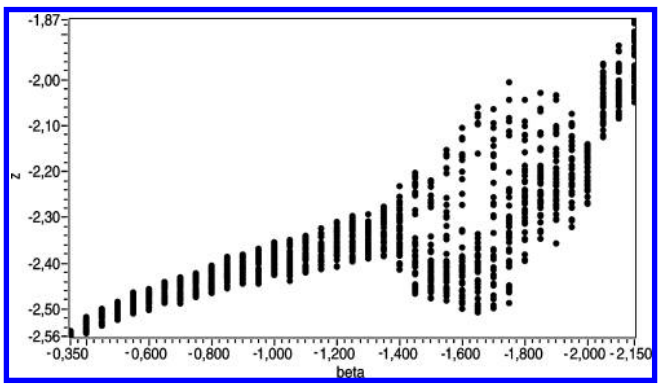

Fig. 16. Experimental bifurcation diagram $z \times \beta$ for $\alpha = -4.00$.

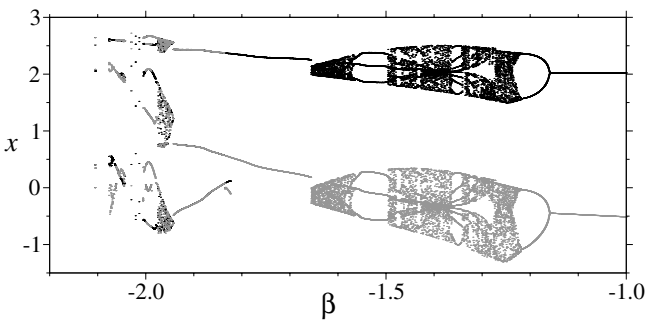

Fig. 17. Theoretical bifurcation diagram $x \times \beta$ for $\alpha = -4.00$.

reproduce the parameter values of the theoretical system. It is worth to comment that the attractor parameters match the attractor region in the parameter space shown in Fig. 6.

6. Conclusion

This work reports some theoretical and experimental investigations related to dynamic behavior of Chua's system with negative parameters, which is still an under-explored side of one of the most studied nonlinear dynamic systems. From a stability analysis using describing functions, the dynamics of this system was outlined in the parameter spaces, which was corroborated by numerical simulations. The study of the negative side of Chua's system parameter space revealed several new structures with interesting characteristics that contrasts to the traditional knowledge about the dynamics of Chua's circuit. For negative parameters, the Shilnikov condition is not satisfied and no Shilnikov scenario is observed. Nonetheless, a rich variety of period-adding cascades and the intense presence of the basin boundary metamorphosis phenomenon, with an important role in the system stability, were discovered. An experimental implementation of Chua's circuit with negative parameters based on electronic analogy was performed, such that the experimental results confirmed the theoretical analysis and simulation results. An interesting topic to be explored in further investigations is the torsion-adding, a phenomenon recently observed where the orbits in period-adding cascades (adding ρ revolutions) also add τ revolutions in the surrounding flow [Medeiros *et al.*, 2013]. Since periodic trajectories in experiments are actually the surrounding flow of the periodic attractor, this phenomenon should play a key role in the study of stability in systems that present intense basin boundary metamorphosis with a great variety of different manifestations of period-adding. Thus, this paper presents new dynamic behaviors and phenomena never observed in Chua's circuit, such that the authors expect that this work stimulates new experimental and theoretical researches to explore deeper the negative side of Chua's circuit parameter space.

Acknowledgments

The authors gratefully acknowledge State of São Paulo Research Foundation (FAPESP), State of Minas Gerais Research Foundation (FAPEMIG), National Counsel of Technological and Scientific Development (CNPq), Coordination for the Improvement of Higher Level -or Education- Personnel (CAPES), and Gorceix Foundation that contributed to the development of this project. The authors also thank the reviewers for their constructive criticisms of the manuscript and Prof. Iberê Luiz Caldas, leader of the Control of Oscillation Group at the Institute of Physics of São Paulo University, for the computational support.

References

Albuquerque, H. A. & Rech, P. C. [2012] "Spiral periodic structure inside chaotic region in parameter-space of a Chua circuit," *Int. J. Circuit Th. Appl.* **40**, 189–194.

Algaba, A., Merino, M. & Rodrígues-Luiz, A. [2012] "Analysis of a Beliakov homoclinic connection with Z_2-symmetry," *Nonlin. Dyn.* **69**, 519–529.

Alligood, K. T., Sauer, T. D. & Yorke, J. A. [1997] *Chaos: An Introduction to Dynamical Systems* (Springer, NY).

Banerjee, T. [2012] "Single amplifier biquad based inductor-free Chua's circuit," *Nonlin. Dyn.* **68**, 565–573.

Barboza, R. [2008] "Hyperchaos in a Chua's circuit with two new added branches," *Int. J. Bifurcation and Chaos* **18**, 1151.

Bartissol, P. & Chua, L. [1988] "The double hook," *IEEE Trans. Circuits Syst.* **35**, 1512–1522.

Bonatto, C. & Gallas, J. A. C. [2007] "Accumulation horizons and period adding in optically injected semiconductor lasers," *Phys. Rev. E* **75**, 055204(R).

Bykov, V. V. [1998] "On bifurcations leading to chaos in Chua's circuit," *Int. J. Bifurcation and Chaos* **8**, 685.

Chua, L. O., Komuro, M. & Matsumoto, T. [1986] "The double scroll family," *IEEE Trans. Circuits Syst.* **33**, 1072–1097.

Cruz, J. M. & Chua, L. O. [1992] "A CMOS IC nonlinear resistor for Chua's circuit," *IEEE Trans. Circuits Syst.-I* **39**, 985–995.

Cruz, J. M. & Chua, L. O. [1993] "An IC chip of Chua's circuit," *IEEE Trans. Circuits Syst.-I* **40**, 614–625.

da Silva, S. L., Rubinger, R. M., de Oliveira, A. G., Ribeiro, G. M. & Viana, E. R. [2009] "Odd periodic window and bifurcations on 2d parameter space of low frequency oscillations," *Physica D* **238**, 1951–1956.

de Souza, S. L. T., Lima, A. A., Caldas, I. L., Medrano-T, R. O. & Guimarães-Filho, Z. O. [2012] "Self-similarities of periodic structures for a discrete model of two-gene system," *Phys. Lett. A* **376**, 1290–1294.

Elwakil, A. S. & Kennedy, M. P. [2000] "Improved implementation of Chua's chaotic oscillator using current feedback op amp," *IEEE Trans. Circuits Syst.-I* **47**, 76–79.

Gaspard, P., Kapral, R. & Nicolis, G. [1984] "Bifurcation phenomena near homoclinic systems: A two-parameter analysis," *J. Stat. Phys.* **35**, 697–727.

Genesio, R. & Tesi, A. [1991] "Chaos prediction in nonlinear feedback systems," *IEE Proc. Contr. Th. Appl.* **138**, 313–320.

Genesio, R. & Tesi, A. [1992] "Harmonic balance methods for the analysis of chaotic dynamics in nonlinear systems," *Automatica* **28**, 531–548.

Glad, T. & Ljung, L. [2000] *Control Theory — Multivariable and Nonlinear Methods* (Taylor & Francis).

Grebogi, C., Ott, E. & Yorke, J. A. [1987] "Basin boundary metamorphoses: Changes in accessible boundary orbits," *Physica D* **24**, 243–262.

Guckenheimer, J. & Holmes, P. [1983] *Nonlinear Oscillation, Dynamical Systems, and Bifurcations of Vector Fields* (Springer-Verlag, NY).

Hoff, A., da Silva, D. T., Manchein, C. & Albuquerque, H. A. [2014] "Bifurcation structures and transient chaos in a four-dimensional Chua model," *Phys. Lett. A* **56**, 171–177.

Kaneko, K. [1982] "On the period-adding phenomena at the frequency locking in a one-dimensional mapping," *Prog. Theor. Phys.* **68**, 669–672.

Kennedy, M. P. [1992] "Robust op-amp realization of Chua's circuit," *Frequenz* **46**, 66–88.

Khalil, H. [1996] *Nonlinear Systems* (Prentice-Hall Inc.).

Kiliç, R., Alçi, M., Çam, U. & Kuntman, H. [2002] "Improved realization of mixed-mode chaotic circuit," *Int. J. Bifurcation and Chaos* **12**, 1429.

Komuro, M., Tokunaga, R., Matsumoto, T., Chua, L. O. & Hotta, A. [1991] "Global bifurcation analysis of the double scroll circuit," *Int. J. Bifurcation and Chaos* **1**, 139.

Lahiri, A. & Gupta, M. [2011] "Realizations of grounded negative capacitance using CFOAs," *Circuits Syst. Sign. Process.* **30**, 143–155.

Madan, R. N. [1993] *Chua's Circuit: A Paradigm for Chaos* (World Scientific, Singapore).

Matsumoto, T. [1984] "A chaotic attractor from Chua's circuit," *IEEE Trans. Circuits Syst.* **31**, 1055–1058.

Matsumoto, T., Chua, L. O. & Komuro, M. [1985] "The double scroll," *IEEE Trans. Circuits Syst.* **32**, 797–818.

Matsumoto, T., Chua, L. O. & Komuro, M. [1986] "The double scroll bifurcations," *Int. J. Circuit Th. Appl.* **14**, 117–146.

Matsumoto, T., Chua, L. O. & Tokunaga, R. [1987] "Chaos via torus breakdown," *IEEE Trans. Circuits Syst.* **34**, 240–253.

Medeiros, E. S., Medrano-T, R. O., Caldas, I. L. & de Souza, S. L. T. [2013] "Torsion-adding and asymptotic winding number for periodic window sequences," *Phys. Lett. A* **377**, 628–631.

Medrano-T, R. O., Baptista, M. S. & Caldas, I. L. [2003] "Homoclinic orbits in a piecewise system and their relation with invariant sets," *Physica D* **15**, 133–147.

Medrano-T, R. O., Baptista, M. S. & Caldas, I. L. [2005] "Basic structures of the Shilnikov homoclinic bifurcation scenario," *Chaos* **15**, 033112.

Medrano-T, R. O., Baptista, M. S. & Caldas, I. L. [2006] "Shilnikov homoclinic orbit bifurcations in the Chua's circuit," *Chaos* **15**, 043119.

Medrano-T, R. O. & Caldas, I. L. [2010] "Periodic windows distribution resulting from homoclinic bifurcations in the two-parameter space," arXiv:1012.2241.

Moon, F. C. & Li, G.-X. [1985] "Fractal basin boundaries and homoclinic orbits for periodic motion in a two-well potential," *Phys. Rev. Lett.* **55**, 1439–1442.

Morgül, Ö. [1995] "Inductorless realization of Chua oscillator," *Electron. Lett.* **31**, 1403–1404.

Neymeyr, K. & Seelig, F. [1991] "Determination of unstable limit cycles in chaotic systems by method of unrestricted harmonic balance," *Z. Naturforsch. A* **46**, 499–502.

Ogata, K. [1970] *Modern Control Engineering* (Prentice-Hall, NJ).

Oliveira, N., Kienitz, K. & Misawa, E. [2012] "A describing function approach to the design of robust limit-cycle controllers," *Nonlin. Dyn.* **67**, 357–363.

Ott, E. [1993] *Chaos in Dynamical Systems* (Cambridge University Press, NY).

Rech, P. C. [2013] "Nonlinear dynamics investigation in parameter planes of a periodically forced compound KdV-Burgers equation," *Eur. Phys. J. B* **86**, 356.

Robert, C., Alligood, K. T., Ott, E. & Yoke, J. A. [2000] "Explosions of chaotic sets," *Physica D* **144**, 44–61.

Rocha, R., Martins-Filho, L. & Machado, R. [2006] "A methodology for the teaching of dynamical systems using analogous electronic circuits," *Int. J. Electr. Eng. Educ.* **43**, 334–345.

Rocha, R. & Medrano-T, R. O. [2009] "An inductor-free realization of the Chua's circuit based on electronic analogy," *Nonlin. Dyn.* **56**, 389–400.

Rocha, R., Andrucioli, G. L. D. & Medrano-T, R. O. [2010] "Experimental characterization of nonlinear systems: A real-time evaluation of the analogous Chua's circuit behavior," *Nonlin. Dyn.* **62**, 237–251.

Rodriguez-Vazquez, A. & Delgado-Restituto, M. [1993] "CMOS design of chaotic oscillators using state variables: A monolithic Chua's circuit," *IEEE Trans. Circuits Syst.-II* **40**, 596–613.

Savacı, F. A. & Günel, S. [2006] "Harmonic balance analysis of the generalized Chua's circuit," *Int. J. Bifurcation and Chaos* **16**, 2325–2332.

Senani, R. & Gupta, S. S. [1998] "Implementation of Chua's chaotic circuit using current feedback op-amps," *Electron. Lett.* **34**, 829–830.

Shilnikov, L. P. [1965] "A case of existence an enumerable set of periodical motions," *Sov. Math. Dokl.* **6**, 163–166.

Slotine, J.-J. E. & Li, W. [1991] *Applied Nonlinear Control* (Prentice-Hall Inc.).

So, P., Luke, T. B. & Barreto, E. [2014] "Networks of theta neurons with time-varying excitability: Macroscopic chaos, multistability, and final-state uncertainty," *Physica D* **267**, 16–26.

Stegemann, C. & Rech, P. C. [2014] "Organization of the dynamics in a parameter plane of a tumor growth mathematical model," *Int. J. Bifurcation and Chaos* **24**, 1450023.

Swamy, M. [2011] "Mutators, generalized impedance converters and inverters, and their realization using generalized current conveyors," *Circuits Syst. Sign. Process.* **30**, 209–232.

Tôrres, L. A. B. & Aguirre, L. A. [2000] "Inductorless Chua's circuit," *Electron. Lett.* **36**, 1915–1916.

Trejo-Guerra, R., Tlelo-Cuautle, E., Sánchez-López, C., Muñoz-Pacheco, J. M. & Cruz-Hernández, C. [2010] "Realization of multiscroll chaotic attractors by using current-feedback operational amplifiers," *Rev. Mex. Fís.* **56**, 268–274.

Weldon, T. P. [1990] "An inductorless double scroll chaotic circuit," *Amer. J. Phys.* **58**, 936–941.

Zhong, G. Q. & Ayrom, F. [1985] "Experimental confirmation of chaos from Chua's circuit," *Int. J. Circuit Th. Appl.* **13**, 93–98.